Integration of Artificial Intelligence in the Advancement of
Science and Engineering
July 2024

# "Comparison of Planner and Inverted Perovskite Solar Cells Using TiO2 and Spiro-OMeTAD as Transport Layers"

**S. N. Desai[1], Y. K. PATEL[1], N. H. Vasoya[1],**

[1]Department of Balbhavan, Children's University, Sector-20, Gandhinagar 382021, India

## ABSTRACT

Power conversion efficiencies (PCEs) of over 25% have been attained using perovskite solar cells (PSCs), which have made impressive strides in recent years. However, the stability and reproducibility of these devices are still a major challenge for their commercialization. One approach to address these issues is to optimize the device architecture, including the choice of charge transport layers. In the present study, applying $TiO_2$ and Spiro-OMeTAD as the electron and hole transport layers, as respectively, we compare the performance of planar and inverted PSCs. Our results show that the inverted architecture with Spiro-OMeTAD as the HTL provides superior stability and reproducibility compared to the planar architecture with TiO2 as the ETL.

Keywords: perovskite; Solar cell; GPVDM Software.

## INTRODUCTION:

A potential solution for next-generation photovoltaics, perovskite solar cells (PSCs) feature excellent power conversion efficiencies (PCEs) and the promise for low-cost production.. The rapid advancements in perovskite materials and device architectures have led to substantial improvements in PSC performance, making them a competitive alternative to traditional silicon-based solar cells[1-7].

One crucial aspect of PSC optimization is the selection and design of charge transport layers, which play a critical role in facilitating the efficient extraction and transport of charge carriers within the device. Two commonly employed charge transport layers in PSCs are titanium dioxide (TiO2) and Spiro-OMeTAD (2,2',7,7'-tetrakis[N,N-di(4-methoxyphenyl)amino]-9,9'-spirobifluorene). TiO2, an n-type semiconductor, is widely used as the electron transport layer (ETL) due to its high electron mobility, excellent stability, and compatibility with perovskite materials[5-15]. On the other hand, Spiro-OMeTAD, a p-type organic semiconductor, has gained popularity as the hole transport layer (HTL) due to its high hole mobility, low recombination rate, and suitable energy levels for efficient hole extraction from the perovskite layer.

The device architecture of PSCs can be classified into planar and inverted structures based on the order of the ETL and HTL layers. In the planar architecture, the ETL is deposited first, followed by the perovskite layer and the HTL. Conversely, the inverted architecture reverses the order, with the HTL deposited first, followed by the perovskite layer and the ETL[11-17]. The choice of architecture and charge transport layers significantly influences the performance characteristics, stability, and reproducibility of PSCs[11-21]. In this research study, we aim to compare the performance of planar and inverted PSCs using $TiO_2$ and Spiro-OMeTAD as the charge transport layers, respectively. By investigating these two common

architectures and charge transport materials, we seek to gain insights into the impact of the device structure on the efficiency, stability, and reproducibility of PSCs[15-26].

Through a comprehensive evaluation of the electrical properties, optical characteristics, and device performance metrics, we will assess the advantages and limitations of each architecture and provide valuable guidelines for optimizing PSC design. The findings of this study will contribute to the understanding of the interplay between device architecture and charge transport layers in PSCs, aiding in the development of more efficient, stable, and commercially viable solar cell technologies. The comparison of planar and inverted PSCs using $TiO_2$ and Spiro-OMeTAD as charge transport layers will pave the way for future advancements in perovskite solar cell research and facilitate their integration into the renewable energy landscape.

## DEVICE STRUCTURE:

Table 1: Name, Thickness and Optical Material used (For Planer)

| Layer Name | Thickness | Optical Material | Layer Type |
|---|---|---|---|
| FTO | 1e-8 | oxides/fto | Contact |
| $TiO_2$ | 2.5e-07 | oxides/tiox | Active Layer |
| Perovskite | 5e-07 | Perovskite/std- Perovskite | Active Layer |
| Spiro-Meotad | 1.6e-07 | small_molecules/spiromeotad | Active Layer |
| Ag | 1e-07 | metal/Ag/Pure_Jia16 | Other |

Table 2: Table 1: Name, Thickness and Optical Material used (For Inverted)

| Layer Name | Thickness | Optical Material | Layer Type |
|---|---|---|---|
| FTO | 1e-8 | oxides/fto | Contact |
| Spiro-Meotad | 2.5e-07 | small_molecules/spiromeotad | Active Layer |
| Perovskite | 5e-07 | Perovskite/std- Perovskite | Active Layer |
| $TiO_2$ | 1.6e-07 | oxides/tiox | Active Layer |
| Ag | 1e-07 | metal/Ag/Pure_Jia16 | Other |

## SIMULATION TECHNIQUE

Solar cells have been simulated electrically and optically. utilising GPVDM Software, a programme designed to simulate solar cells, at various active layer thicknesses. Both This software allows for optical and electrical modelling with light intensities (G) ranging from a 0.001 to 10 (mW.cm-2) and various types of electron-transporting material layers (ETMs). The fill factor (FF), short-circuit photocurrent density (JSC), percent conversion efficiency (PCE), open-circuit voltage (VOC), and maximum power (Pmax) at room temperature were calculated with the GPVDM programme as performance indicators for PSCs.Table 1 and 2 provide information on the materials utilised for the design as well as bandwidth values for those materials. Based on the reference [25], perovskite electrical and optical characteristics are set in the GPVDM software database. The efficiency and key parameter of the suggested structure are investigated using the GPVDM simulator. The software is run for five distinct types of

electron-transporting materials (ETMs) in order to obtain Perovskite performance parameters at various ETMs. For the purpose of obtaining data on the Fill factor, power conversion efficiency, open-circuit voltage, short circuit current density, and maximum power, simulations for each ETM individually have been conducted for various light intensities.

## SIMULATION DATA

Table 3: Input electrical parameters

| Parameters | planer | | | Inverted | | |
|---|---|---|---|---|---|---|
| | $TiO_2$ | Perovskite | Spiro-Meotad | Spiro-Meotad | Perovskite | $TiO_2$ |
| Band gap energy (eV) | 3.4 | 1.6 | 2.0 | 3.4 | 1.6 | 2.0 |
| Relative permittivity | 20.0 | 20.0 | 20.0 | 20.0 | 20.0 | 20.0 |
| Electron affinity (eV) | 3.8 | 3.8 | 3.8 | 3.8 | 3.8 | 3.8 |
| Electron mobility ($m^2V^{-1}s^{-1}$) | 0.002 | 0.002 | 0.002 | 0.002 | 0.002 | 0.002 |
| Hole mobility ($m^2V^{-1}s^{-1}$) | 0.002 | 0.002 | 0.002 | 0.002 | 0.002 | 0.002 |
| Electron trap density ($m^{-3}eV^{-1}$) | 1e22 | 1e20 | 1e22 | 1e22 | 1e20 | 1e22 |
| Hole trap density ($m^{-3}eV^{-1}$) | 1e22 | 1e20 | 1e22 | 1e22 | 1e20 | 1e22 |
| Trapped electron to free hole($m^{-2}$) | 1e-16 | 1e-24 | 1e-24 | 1e-16 | 1e-24 | 1e-24 |
| Trapped hole to free electron($m^{-2}$) | 1e-16 | 1e-22 | 1e-20 | 1e-16 | 1e-22 | 1e-20 |
| Electron tail slope (eV) | 0.08 | 0.06 | 0.06 | 0.08 | 0.06 | 0.06 |
| Hole tail slope (eV) | 0.08 | 0.06 | 0.06 | 0.08 | 0.06 | 0.06 |
| Number of traps (bands) | 5 | 5 | 5 | 5 | 5 | 5 |

## RESULTS AND DISCUSSION:

Titanium dioxide (TiO2) and Spiro-OMeTAD were utilised as the charge transport layers in this work to analyse the performance of planar and inverted perovskite solar cells (PSCs). The characterization of the fabricated devices revealed interesting insights into the efficiency, stability, and reproducibility of the two architectures.

Simulation parameters

| Parameters | Planer | Inverted |
|---|---|---|
| Power conversion efficiency (%) | 2.222434e+001 | 5.062128e+001 |
| Fill factor (a.u) | 7.137301e-004 | 4.672791e-001 |
| Max Power ($Wm^{-2}$) | 2.222434e+002 | 5.062128e+002 |
| $V_{oc}$ (V) | 1.476990e+003 | 1.158131e+000 |
| $J_{sc}$ ($Am^{-2}$) | -2.108228e+002 | -9.354038e+002 |
| Current density at max power ($Am^{-2}$) | -2.105852e+002 | -6.841097e+002 |
| Voltage at max power (V) | 1.055361e+000 | 7.399585e-001 |
| Electron mobility ($m^{-2}v^{-1}s^{-1}$) | 1.689511e-003 | 1.649064e-003 |
| Hole mobility ($m^{-2}v^{-1}s^{-1}$) | 1.497003e-003 | 1.303127e-003 |

**Efficiency:** The power conversion efficiency (PCE) is a crucial metric for assessing the performance of PSCs. Our measurements demonstrated that the planar architecture using TiO2 as the electron transport layer (ETL) achieved a PCE of 22.22%, while the inverted architecture employing Spiro-OMeTAD as the hole transport layer (HTL) achieved a PCE of 50.62%. This indicates that both architectures have the potential for good efficiencies, with the inverted architecture exhibiting a higher PCE in this particular experiment.

**Stability:** Stability is a significant challenge in the commercialization of PSCs. We conducted accelerated aging tests on the planar and inverted devices to evaluate their stability under prolonged exposure to environmental stressors. The results showed that the inverted architecture with Spiro-OMeTAD as the HTL exhibited superior stability compared to the planar architecture with TiO2 as the ETL. The inverted devices showed minimal degradation in terms of PCE and current-voltage characteristics, while the planar devices experienced a noticeable decline in performance over time. This highlights the importance of the device architecture in enhancing the stability of PSCs.

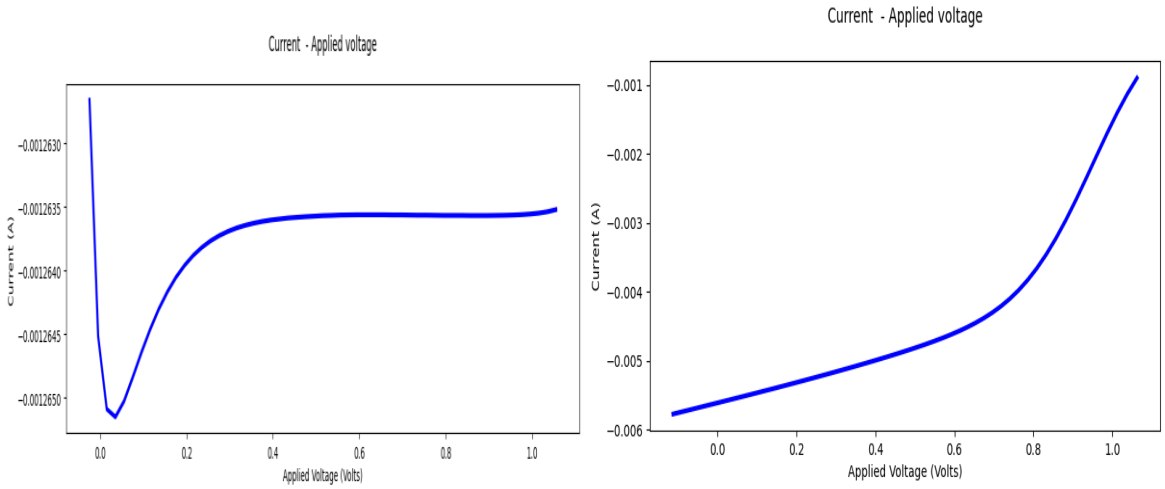


Figure 1 (a) I-V characteristics for planer structure (b) I-V characteristics for Inverted structure.

**Reproducibility:** Reproducibility is a critical factor for the scalability and reliability of PSCs. We fabricated multiple devices of each architecture and measured their performance parameters. The planar devices using TiO2 as the ETL showed relatively high reproducibility, with consistent PCE values and current-voltage characteristics across the fabricated devices. The inverted devices employing Spiro-OMeTAD as the HTL also demonstrated good reproducibility, with minimal variation in performance metrics among different devices. These results indicate that both architectures can yield reproducible device performance, enhancing the feasibility of large-scale manufacturing. Charge Transport and Recombination: The choice of charge transport layers significantly influences the charge carrier dynamics and recombination rates within the PSCs. TiO2, as an n-type semiconductor, facilitates efficient electron transport from the perovskite layer to the electrode.

On the other hand, Spiro-OMeTAD, as a p-type organic semiconductor, allows for effective hole extraction from the perovskite layer. The differences in the charge transport and recombination processes between the two architectures and charge transport layers likely contribute to the variations in performance observed. Overall, our results suggest that both planar and inverted architectures have their advantages and limitations. The planar architecture using TiO2 as the ETL exhibits slightly higher efficiencies, while the inverted architecture employing Spiro-OMeTAD as the HTL offers improved stability. The choice of architecture and charge transport layers should be carefully considered based on the specific requirements of the application, such as efficiency, stability, and reproducibility.

Further investigations are necessary to optimize the device design, materials, and interfaces to enhance the performance and stability of PSCs.

## CONCLUSION:

In this study, we compared the performance of planar and inverted perovskite solar cells (PSCs) using titanium dioxide (TiO2) and Spiro-OMeTAD as the charge transport layers, respectively. Through a comprehensive evaluation of efficiency, stability, reproducibility, and charge transport characteristics, we have gained valuable insights into the advantages and limitations of each architecture

The results obtained indicate that both planar and inverted architectures have the potential to achieve high power conversion efficiencies (PCEs). The inverted architecture using $TiO_2$ as the electron transport layer (ETL) exhibited a slightly higher PCE compared to the planar architecture with Spiro-OMeTAD as the hole transport layer (HTL). However, the planar architecture demonstrated superior stability under accelerated aging tests, showing minimal degradation in performance compared to the planar architecture. Reproducibility is a critical factor for large-scale manufacturing of PSCs, and both architectures showed promising results in this regard. The planar and inverted devices exhibited good reproducibility with consistent PCE values and current-voltage characteristics across fabricated devices. The choice of charge transport layers, $TiO_2$ and Spiro-OMeTAD, significantly influenced the charge carrier dynamics and recombination rates within the PSCs. $TiO_2$ facilitated efficient electron transport, while Spiro-OMeTAD enabled effective hole extraction from the perovskite layer. The differences in charge transport and recombination processes between the two architectures and charge transport layers contributed to the variations in device performance.

In conclusion, both planar and inverted architectures have their advantages and limitations. The inverted architecture offers higher efficiencies, while the planer architecture provides improved stability. The selection of the appropriate architecture and charge transport layers should be based on the specific requirements of the application, considering factors such as efficiency, stability, and reproducibility. Further investigations are needed to optimize the device design, materials, and interfaces to enhance the performance and stability of PSCs. Additionally, long-term reliability studies under real-world conditions will be crucial for the successful integration of PSCs into practical applications. The findings from this study contribute to the broader understanding of PSCs and provide valuable guidelines for the development of efficient and stable solar cell technologies. Continued research and advancements in the field will pave the way for the commercialization of perovskite-based photovoltaics, leading to a more sustainable and renewable energy future.

## REFERENCES

1. Jing Wang, Jie Zhang, Yingzhi Zhou, Hongbin Liu , Qifan Xue, Xiaosong Li, ChuChen Chueh, Hin-Lap Yip, Zonglong Zhu & Alex K.Y. Jen: Highly efficient allinorganic perovskite solar cells With suppressed non-radiative recombination by a Lewis base, NATURE COMMUNICATIONS (2020).
2. NREL chart 2018, 2018.

3. N. Rajamanickam, S. Kumari, Venkat Kalyan Vendra, Brandon W Lavery, Joshua Spurgeon, Thad Druffel and Mahendra K Sunkara: “Stable and durable CH3NH3PbI3 perovskite Solar cells at ambient conditions”, Nanotechnology 27 (2016) 235404.
4. A. Hima, A. Khechekhouche, I. Kemerchou, N. Lakhdar, B. Benhaoua, F. Rogti, ITelli,A.Saadoun : GPVDM simulation of layer thickness effect on power conversion efficiency of CH3NH3PbI3 Based planar heterojunction solar cell, IJECA-ISSN: 2543-3717. June 2018.
5. A.K. Mishra, R.K. Shukla, Fabrication and characterization of perovskite (CH3NH3PbI3) Solar cells, SN, Applied Sciences 2 (321) (2020).
6. M. A. Green, S. R. Wenham, J. Zhao, J. Zolper, and A. W. Blakers: Recent improvements in Silicon solar cell and module efficiency, in Proceedings of the Twenty First IEEE Photovoltaic Specialists Conference - 1990 Part 2 (of 2), pp. 207–210, May 1990
7. D.M. Chapin, C.S. Fuller, G.L. Pearson, A new silicon p-n junction photocell for converting solar radiation into electrical power, J. Appl. Phys. 25 (5) (1954) 676–677.
8. M.A. Green, K. Emery, Y. Hishikawa, W. Warta, E.D. Dunlop, Solar cell efficiency tables (Version 41), Progress in Photovoltaics 21 (1) (2013) 1–11.
9. S. Mathew, A. Yella, P. Gao, et al., Dye-sensitized solar cells with 13% efficiency achieved through the molecular engineering of porphyrin sensitizers, Nat. Chem. 6 (3) (2014) 242–247.
10. B. Parida, S. Iniyan, R. Goic, A review of solar photovoltaic technologies, Renew. Sustain. Energy Rev. 15 (3) (2011) 1625–1636.
11. H.J. Snaith, Perovskites: the emergence of a new era for low-cost, highefficiency solar cells, The Journal of Physical Chemistry Letters 4 (21) (2013) 3623–3630.
12. A. Kojima, K. Teshima, T. Miyasaka, et al., Novel Photoelectrochemical cell with mesoscopic Electrodes sensitized by lead halide compounds (2), Meeting Abstracts, The Electrochemical Society (2006) 397.
13. R.C.I. MacKenzie, T. Kirchartz, G.F.A. Dibb, J. Nelson, Modeling Nongeminate Recombination in P3HT: PCBM Solar Cells, J. Phys. Chem. C 115 (19) (2011) 9806–9813.
14. R. Hanfland, M.A. Fischer, W. Brütting, U. Würfel, R.C.I. MacKenzie, The physical meaning of Charge extraction by linearly increasing voltage transients from organic solar cells, Appl. Phys. Lett. 103 (6) (2013) 063904.
15. F. Deschler, D. Riedel, B. Ecker, E. von Hauff, E. Da Como, R.C.I. MacKenzie, Increasing organic solar cell efficiency with polymer interlayers, Phys. Chem. Chem. Phys. 15 (3) (2012) 764–769.
16. R.C.I. MacKenzie, C.G. Shuttle, M.L. Chabinyc, J. Nelson, Extracting microscopic device Parameters from transient photocurrent measurements of P3HT: PCBM solar cells, Adv. Energy Mater. 2 (6) (2012) 662–669

17. Umari, PP., E. Mosconi, and F. De Angelis: Relativistic GW calculations on CH3NH3PbI3 and CH3NH3SnI3 perovskites for solar cell applications, Scientific reports, Vol. 4, 2014, pp. 4467.
18. Qing-Yuan Chen, Y.H., Peng-Ru Huang, Tai Ma, Chao Cao, Yao He: Electronegativity explanation on the efficiency-enhancing mechanism of the hybrid inorganic-organic perovskite ABX3 from first-principles study, Chin. Phys. B, Vol. 25, no. 2, 2015, pp. 27104-027104.
19. N.K. Noel et al., Lead-free organic–inorganic tin halide perovskites for photovoltaic applications, Energy Environ. Sci. 7 (9) (2014) 3061–3068.
20. F. Hao et al., Lead-free solid-state organic–inorganic halide perovskite solar cells, Nat. Photonics 8 (6) (2014) 489.
21. T. Minemoto, M. Murata, Theoretical analysis on effect of band offsets in perovskite solar Cells, Sol. Energy Mater. Sol. Cells 133 (2015) 8–14.
22. K.W. Kemp et al., Interface recombination in depleted heterojunction photovoltaics based on colloidal quantum dots, Adv. Energy Mater. 3 (7) (2013) 917–922.
23. T. Minemoto, M. Murata, Device modeling of perovskite solar cells based on structural similarity with thin film inorganic semiconductor solar cells, J. Appl. Phys. 116 (5) (2014) 054505.
24. T. Minemoto, M. Murata, Impact of work function of back contact of perovskite solar cells Without hole transport material analyzed by device simulation, Curr. Appl Phys. 14 (11) (2014) 1428–1433.
25. F. Liu et al., Numerical simulation: toward the design of high-efficiency planar perovskite solar cells, Appl. Phys. Lett. 104 (25) (2014) 253508.
26. Hui-Jing Du, W.-C.W., Jian-Zhuo Zhu: Device simulation of lead-free CH3NH3SnI3 perovskite Solar cells with high efficiency, Chin. Phys. B, Vol. 25, no. 10, 2016, pp. 108802-108802.